A Model-Driven Approach to Microwave Diagnostics in Biomedical Applications

Salvatore Caorsi, Gian Luigi Gragnani, *Member, IEEE*,
Matteo Pastorino, *Senior Member, IEEE*, and Mauro Rebagliati

***Abstract*—In this paper, a model-driven approach to microwave diagnostics for biological bodies is presented. The approach is developed in the space domain and is based on a numerical solution of the equation for the scalar two-dimensional (2-D) inverse-scattering problem. The aim is to use "a prior" information on the biological body under test (homogeneous along the transverse axis) in order to focus the investigation process on only one subdomain of the body, with a considerable computational saving. The method requires the numerical computation of the Green's function for an unperturbed model of the body in order to apply reconstruction techniques to a reduced investigation domain, which can be changed inside the body, with a reduction in on-line computation. The paper defines the mathematical formulation for a 2-D TM and presents the reconstructions of some schematized scatterers corresponding to living tissues.**

I. Introduction

THE USE OF microwaves for diagnostic purposes in biomedical applications is a very challenging topic. Even though about ten years have elapsed since the publication by Larsen and Jacobi [1], microwave imaging does not seem to be competitive with other diagnostic techniques, for instance, CT, ultrasounds, nuclear magnetic resonance, and positron emission. Nevertheless, microwave imaging has many potential advantages. First of all, it allows one to obtain the distribution of the complex dielectric permittivity of a tissue; this is basic information that would not be acquired by using other diagnostic techniques [2]. From such distribution, some researchers try to derive other important medical and biological information (e.g., gradients in water contents, blood-flow rates, etc.) to obtain noninvasive dosimetry and to measure power deposition in order to evaluate biohazards due to undesired exposure [3]. Moreover, the technology required has reached a high degree of development, as it is also used for telecommunications. Therefore, it could be much more economical, more reliable, and safer (for both patients and physicians) than the technology used for some other techniques currently applied. In addition, microwave imaging could allow one to overcome the limitations of other techniques; for instance, it could be possible to apply it to large discontinuities (ultrasounds, for example, are applied to small discontinuities) and to low tissue densities (X-rays require higher densities).

Manuscript received October 20, 1995; revised February 16, 1996.

S. Caorsi is with the Department of Electronics, University of Pavia, 27100 Pavia, Italy.

G. L. Gragnani, M. Pastorino, and M. Rebagliati are with the Department of Biophysical and Electronic Engineering, University of Genoa, 16145 Genova, Italy.

Publisher Item Identifier S 0018-9480(96)07036-6.

Many papers on this topic can be found in the literature. For instance, it is worth mentioning the review works [4]–[7], which provide a large number of references that could not be cited in this paper.

The research on microwave imaging pursues two main lines: 1) study of efficient illumination and measurement systems; and 2) development of suitable algorithms for dielectric reconstruction. These are the two basic issues. Experts in image processing (which is not a secondary task) provide the tools for extracting image parameters and enhancing the crude images obtained by the inverse-scattering process.

This paper is focused on aspects related to point 2), for which the state-of-the-art, in particular, the obtained reconstructions, cannot yet be considered completely satisfactory; this often leads to regard microwave imaging as a technique that is still in its *infancy* [8].

Even though very interesting results were obtained in the past by using algorithms developed in the frequency domain [2], [9] (based on the so-called Fourier Diffraction Theorem), two main limitations (i.e., the low resolution that can be obtained according to the Rayleigh criterion and the high contrast of a biological body) have led to the prefered space-domain techniques [3], [10]–[14], [15] or to frequency-domain reconstructions as initial guesses for space-domain iterative approaches [6], [16].

Unfortunately, algorithms developed in the space domain still exhibit some limitations. They are based on integral equations, usually solved after discretization of a continuous model. For example, in 1991, we developed a multi-illumination multiview approach in which the electromagnetic source rotates jointly with the observation domain around the body under test [17]. The approach was based on the pseudoinversion transformation previously applied successfully in [11]. However, the limitations inherent in transforming the inverse-scattering problem into an inverse-source problem, however, make this approach very ill-posed, unstable, and very sensitive to configuration parameters [18].

This is the reason why current inverse-scattering algorithms redefine the problem as an optimization problem that can be solved by associating the information provided by the integral equation for the internal field with *a priori* information on the model. Minimization procedures are used. Nevertheless, the resulting problem is usually highly nonlinear and the solution becomes more and more complex. For example, the iterative techniques based on the Newton-Kantorovich method yield satisfactory results [19], [20], which constitute a significant improvement over previously reported reconstructions. The

space-domain methods developed, however, allow one to obtain discretizations that are far from providing accuracies that can be compared with those obtainable with other diagnostic techniques. Moreover, in our opinion, algorithms that at each iteration step require the solution of a direct-scattering problem are very stable, but involve too high a computational load.

In [21], we proposed an iterative method based on a probabilistic approach with extensive use of *a priori* information. As compared with other techniques, this method allowed larger discretizations (on the order of 10 000 cells). Unfortunately, the simulated annealing technique used required a large amount of computation, even though the *a priori* information inserted in the Markov-Random-Field model considered made the convergence rate of the approach much faster than it would have been if simulated annealing had been applied directly to the rough discretized model.

On the other hand, can one expect to obtain images rapidly, with high resolution and fine details, by starting from a complex nonlinear electromagnetic model, often very ill-posed and in the presence of high contrast? In our opinion, the best solution lies in fully exploting *a priori* information in the model and, if possible, in integrating the microwave technique with other traditional diagnostic techniques.

The basic idea of the proposed approach is the following: it may be important to investigate, for diagnostic purposes, only a subregion of a biological body, or, in general, of the human body, and such a subregion can correspond to one or more organs. On the contrary, the microwave-imaging techniques so far proposed consider a whole biological body as the investigation domain. Therefore, they do not allow one to focus the investigation on a smaller domain. The present paper describes an imaging approach (based on the integral equations) that uses the model of a biological body as *a priori* information in order to restrict the investigation domain to a subregion of the body. The scatterer to be detected is only defined by differences in the distributions of the dielectric parameters between the actual biological body and the assumed model of the subregion. The basic idea of this approach was preliminarily presented in [22]. The approach is developed in two steps: 1) computation (in discretized form) of the Green's function for the inhomogeneous structure corresponding to the assumed model of the biological body and 2) solution of a direct scattering problem to determine the field distribution (due to the incident field) inside this structure. Given the model structure, the two steps are accomplished off line, once and for all.

At this point, one of the previously described reconstruction algorithms can be applied to a restricted investigation region. As the investigation domain remains small, we can exploit all the available computational resources for only the part under test, for which it is possible to obtain a better resolution. In addition, the shape and the position of the restricted investigation domain can be moved inside the scene in order to consider a different subregion of interest inside the body, but the on-line computation is not very heavy. Moreover, the range of applicability of the Born approximation [23] can be extended to bodies for which the "excess of permittivity" is weak with respect to the model structure but not necessarily with respect to the infinite background.

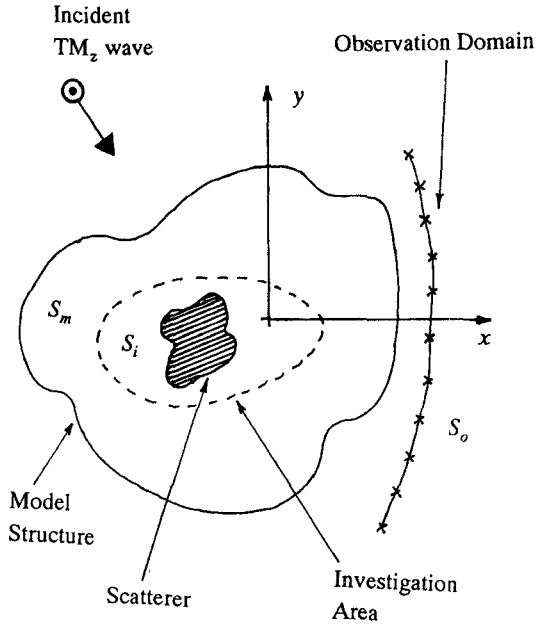

Fig. 1. Cylindrical geometry of the problem.

The paper is organized as follows: In Section II, the mathematical formulation for the approach is defined. In Section III, the possibility of extending the application range of the Born approximation is explored. In Section IV, some numerical results concerning both noiseless and noisy environments are reported that show the capabilities and limitations of the method in providing approximate focalized dielectric reconstructions. Finally, conclusions are drawn in Section V.

II. Theory

Let us consider the infinitely long cylindrical geometry shown in Fig. 1. The cylinder, whose cross section is of arbitrary shape and inhomogeneous, is nonmagnetic and exhibits dielectric features that are invariant in the z direction. The body is illuminated by an incident TM_z-wave electromagnetic field. Plane–wave illumination is not a theoretical requirement. The propagation medium is lossless and homogeneous. Let us define S_o as the observation domain made up of measurement points where the total electric field (the incident field plus the field scattered by the body) is to be recorded. We assume to know the model of the object under test, i.e., the cross section S_m of an object from which the actual body differs only partially. The dielectric permittivity of the model is $\tilde{\varepsilon}_m(x,y)$ and the real unknown permittivity of the object S_m is $\tilde{\varepsilon}_a(x,y)$, where

$$\tilde{\varepsilon}_m(x,y) = \varepsilon_0 \tilde{\varepsilon}_{mr}(x,y) = \varepsilon_0 \left[\varepsilon_{mr}(x,y) - j \frac{\sigma_m(x,y)}{\omega \varepsilon_0} \right] \quad (1)$$

$$\tilde{\varepsilon}_a(x,y) = \varepsilon_0 \tilde{\varepsilon}_{ar}(x,y) = \varepsilon_0 \left[\varepsilon_{ar}(x,y) - j \frac{\sigma_a(x,y)}{\omega \varepsilon_0} \right]. \quad (2)$$

We assume that the differences between the model and the actual biological body are restricted to S_i, i.e., the cross section of an investigation domain. If this hypothesis is not verified, the *excess of permittivity* outside S_i will contribute to the "noise" at the measurement points.

Usually, traditional algorithms require that all discontinuities be contained in the investigation domain (i.e., $S_m \subset S_i$), so the inverse problem is expressed as

$$E_{\text{tot}}(x,y) = E_{\text{inc}}(x,y) + j\omega\mu_0 \iint_{S_i} O(x',y') \times E_{\text{tot}}(x',y')G_0(x,y/x',y')dx'dy' \quad (3)$$

where $G_0(x,y/x',y')$ is the Green's function for free space [23]–[25] and $O(x,y)$ is the object function containing the information about the dielectric properties of the investigation domain S_i.

The various proposed space-domain inversion procedures differ in the way they try to solve (3), which is a nonlinear integral equation with $O(x,y)$ and $E_{\text{tot}}(x,y), (x,y) \in S_i$ as unknowns. Some proposed approaches linearize (3) by suitable approximations [26]–[28] and others reduce the problem to the minimization of nonlinear functionals [16], [29], sometimes using the information given by the integral equation for the electric field inside S_i.

In the present case, the inverse scattering problem is expressed by the following integral equation:

$$E_{\text{tot}}(x,y) = E'_{\text{inc}}(x,y) + j\omega\mu_0 \iint_{S_i} O'(x',y') \times E_{\text{tot}}(x',y')G_m(x,y/x',y')dx'dy' \quad (4)$$

where

$$O'(x,y) = j\omega\varepsilon_0[\tilde{\varepsilon}_{ar}(x,y) - \tilde{\varepsilon}_{mr}(x,y)] \quad (5)$$

$G_m(x,y/x',y')$ is the Green's function for the inhomogeneous model structure and $E'_{\text{inc}}(x,y)$ is the electric field that would be present if S_i showed no variations with respect to the basic configuration. Moreover, in this case, we can usually expect to have $S_i \subset S_m$.

In general, to obtain an adequate solution, it is necessary to use more information; therefore, we use a multi-illumination multiview procedure

$$E^{(v,p)}_{\text{tot}}(x,y) = E'^{(p)}_{\text{inc}}(x,y) + j\omega\mu_0 \iint_{S_i} O'(x',y') \times E^{(v,p)}_{\text{tot}}(x',y')G_m(x,y/x',y')dx'dy' \quad v = 1,\ldots,V, \quad p = 1,\ldots,P \quad (6)$$

where V and P are the numbers of views and illuminations, respectively. For notation simplicity, however, in the following we shall refer to a single-illumination single-view case.

As mentioned in Section I, the problem solution requires two preliminary steps. The first one is the computation of the numerical Green's function. The Green's function for the model cross section is by definition proportional to the field generated at a point (x,y) by an impulsive current density located at (x',y'), so it can be computed by the following integral equation:

$$G_m(x,y/x',y') = G_0(x,y/x',y') + \iint_{S_m} j\omega\varepsilon_0(\tilde{\varepsilon}_{mr}(x'',y'') - 1) \times G_m(x'',y''/x',y')G_0(x,y/x'',y'')dx''dy'' \quad (7)$$

where

$$G_0(x,y/x',y') = -\frac{\omega\mu_0}{4}H_0^{(2)}(k_0\rho) \quad (8)$$

where $H_0^{(2)}(k_0\rho)$ is the Hankel function of the second type and zeroth order, k_0 is the wave number of the incident electric field, and ρ is such that

$$\rho = \sqrt{(x-x')^2 + (y-y')^2}. \quad (9)$$

If the region S_m is partitioned into N_m subdomains, we can obtain $(N_m - 1)$ values of the Green's function for each of the N_m positions at which the impulsive source can be located. Of course, the Green's function is not computed at the point source, as it is infinite, but the contributions of the subdomains containing the source points [25], [30] are taken into account in the discretizing equation (4). Assuming (x_n, y_n) to be the center of the nth subdomain, according to the above discretization, (7) gives N_m algebraic systems of linear equations to be solved

$$[A_k]\underline{\gamma}_k = \underline{g}_k \qquad 1 \le k \le N_m \quad (10)$$

where $\underline{g}_k$ and $\underline{\gamma}_k$ are two arrays of dimensions $(N_m - 1) \times 1$ and are given by $\underline{g}_k(n) = G_0(x_n, y_n/x_k, y_k)$ and $\underline{\gamma}_k(n) = G_m(x_n, y_n/x_k, y_k)$. The Green's matrix $[A_k]$ is of dimensions $(N_m - 1) \times (N_m - 1)$ and its elements are given by

$$a^{(k)}_{p,q} = \delta_{pq} - j\omega\varepsilon_0[\tilde{\varepsilon}_m(x_t, y_t) - 1] \times \iint_{S_t} G_0(x_u, y_u/x', y')dx'dy' \quad (11)$$

where $\delta_{pq} = 0$ if $p \neq q$ and $\delta_{pq} = 1$ if $p = q$; S_t is the tth subdomain and t and u are such that $t = q + \Delta_{qk}$, $u = p + \Delta_{pk}$, as $\Delta_{ij} = 0$ if $i < j$ and $\Delta_{ij} = 1$ if $i \ge j$.

Moreover, in (11) we assume that $\tilde{\varepsilon}_m(x,y)$ is constant inside each subdomain.

Determining the Green's function for all subdomains of the model and for all possible positions of the impulse would require the solution of the N_m algebraic systems (10). Fortunately, we can avoid the impractical solutions of N_m algebraic sistems by deriving the N_m inverse matrices $[A_k]^{-1}$ from the inverse matrix of a matrix $[A]$, which is defined as the matrix from which the generic matrix $[A_k]$ can be derived by deleting the kth row and the kth column. Obviously, the matrix $[A]$ is of dimensions $N_m \times N_m$.

In the following, the above statement is demonstrated. If $a'_{i,k}$ is the ith element of the $k$vth column of $[A]$, we can define an $N_m \times N_m$ matrix $[F]$ whose element is

$$f_{i,J} = \begin{cases} 0 & \text{if } i \neq j \text{ and } j \neq k \\ 1 & \text{if } i = j \text{ and } j \neq k \\ -a'_{i,k}/a'_{k,k} & \text{if } i \neq j \text{ and } j = k \\ 1/a'_{k,k} & \text{if } i = j \text{ and } j = k \end{cases}. \quad (12)$$

Now let us define a matrix $[E]$ such that

$$[E] = [F][A]^{-1}. \quad (13)$$

Now, if we consider the matrix $[E_k]$ obtained by deleting the kth row and the kth column from the matrix $[E]$, the product of $[E_k]$ by $[A_k]$ gives the matrix $[F_k]$, which is equal to the matrix obtained by deleting the kth row and the kth column from $[F]$. This result is consistent with the fact that, by construction, the kth element of the kth column of the matrix $[E]$ is equal to one,

whereas the other elements of the kth column are null. The matrix $[F_k]$, however, is by definition (12) the identity matrix of dimensions $(N_m-1)\times(N_m-1)$. So, after the construction of the matrix $[E]$, obtained by the inversion of the matrix $[A]$, we can derive the N_m matrices $[A_k]^{-1}$ as $[A_k]^{-1}=[E_k]$. It should be noted that the whole computation can be performed off line and only once for a certain model of the biological body and for a given imaging configuration.

The second step of the method is the determination of $E'_{\rm inc}(x,y)$. In (4), $E'_{\rm inc}(x,y)$ is the electric field due to the presence of the unperturbed dielectric characteristics of the model structure that satisfy

$$E'_{\rm inc}(x,y)=E_{\rm inc}(x,y)+\int\!\!\int_{S_m} j\omega\varepsilon_0[\tilde{\varepsilon}_{mr}(x',y')-1] \times E'_{\rm inc}(x',y')G_0(x,y/x',y')dx'dy'. \quad (14)$$

$E'_{\rm inc}(x,y)$ can be determined by solving the direct scattering problem expressed by (14), using any available method for this type of problem. In this paper, the moment method [31] is used, so the solution of (14) is reduced to solving the matrix equation

$$[H]\underline{e}'_{\rm inc}=\underline{e}_{\rm inc} \quad (15)$$

where $[H]$ is an $N_m\times N_m$ Green's matrix and $\underline{e}'_{\rm inc}$ and $\underline{e}_{\rm inc}$ are the numerical arrays that contain the values of $E'_{\rm inc}(x,y)$ and $E_{\rm inc}(x,y)$ in the N_m subdomains of the discretized model configuration. If the same computational scheme as previously used for the numerical computation of G_m is used again, it is evident that $[H]=[A]$, so $[H]^{-1}$ is already available.

If we measure $E_{\rm tot}(x,y)$ in the observation domain, we can express the inverse scattering problem by the integral equation (4). Once the problem has been defined in this way, the solution can be obtained by one of the various inversion methods recently proposed in the literature. In particular, in the present work, we apply the reconstruction technique previously developed by us [17], [21].

III. Born-Type Approximation

Within the classic Born approximation, the total electric field inside the investigation domain is approximated by the known incident electric field, and the external scattered electric field is expressed only in terms of the internal incident electric field $E_{\rm inc}(x,y)$. On the contrary, in an approximate version of the present approach, the total internal electric field is approximated by $E'_{\rm inc}(x,y)$ (i.e., the total field inside the region under test characterized by the *a priori* assumed dielectric permittivity distribution). As previously described, this field can be determined by an off-line computation and can be regarded as an "incident" field for the *excess* of dielectric permittivity due to the difference, inside the investigation domain, between the actual object and the ideal object. In this sense, the approximation used exhibits some analogies to the Born approximation. Within this Born-type approximation, for $(x,y)\in S_i$, (3) is linearized and one can derive directly the distributions of the dielectric parameters.

This approach expands the range of applicability of the Born approximation, as it does not require that the scatterer be weak with respect to the propagation medium but only with respect to the surrounding medium. This fact can be evaluated in the following simple test case. The reader can also take advantage of [32].

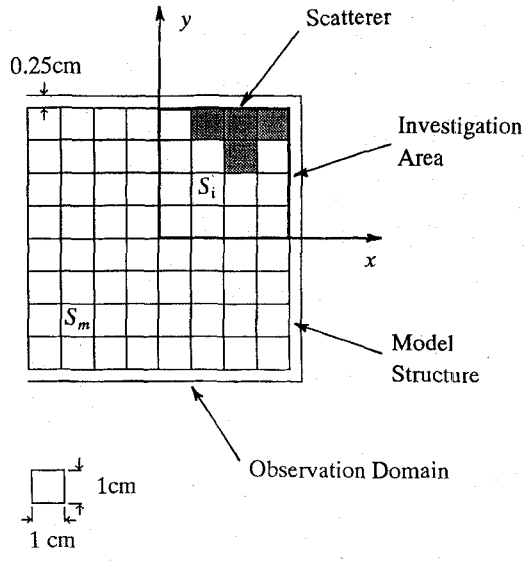

Fig. 2. Geometrical configuration for a test case.

Let us consider the lossless cylinder in Fig. 2. The square cross section is partitioned into 64 square cells, 16 of which are assumed to make up the investigation domain. The measurement points are 65 and the propagation medium is characterized by ε_0 and μ_0. The incident field is a unit uniform transverse-magnetic (TM) plane wave whose direction of propagation is the x axis and whose frequency is 1 GHz. The figure shows a *variation* in the dielectric permittivity (shaded area) with respect to the model. This *excess of permittivity* is regarded as the *scatterer* to be detected.

For the configuration in Fig. 2, we consider an *excess* of dielectric permittivity ($\varepsilon_{ar}=2$) for the basic model structure whose dielectric permittivity is $\varepsilon_{mr}=1.5$. We want to test the approximate approach by using data affected by noise. Fig. 3 gives the errors on the reconstructions of the relative dielectric permittivity for different values of the signal-to-noise ratio, in the case in which Gaussian noise is added to the values of the measured field in order to simulate more realistic operating conditions. The figure shows that, even for small enough signal-to-noise ratios, the errors both on the scatterer and on the remaining "empty" part of the investigation domain are limited. Moreover, the error values obtained by the Born-type version for both the scatterer and the "empty" domain do not differ too much from those obtained by the complete approach.

Then we want to see how the chosen permittivity value of the scatterer affects the reconstructions of both the scatterer and the "empty" domain. The values of the *excess of permittivity* are changed. Fig. 4 gives the errors on the reconstructed relative dielectric permittivity versus some values of the permittivity of the internal scatterer. It can be noticed that the errors related to the modified version are only slightly larger than those related to the complete approach. To verify the validity of the Born-type approximation in those cases

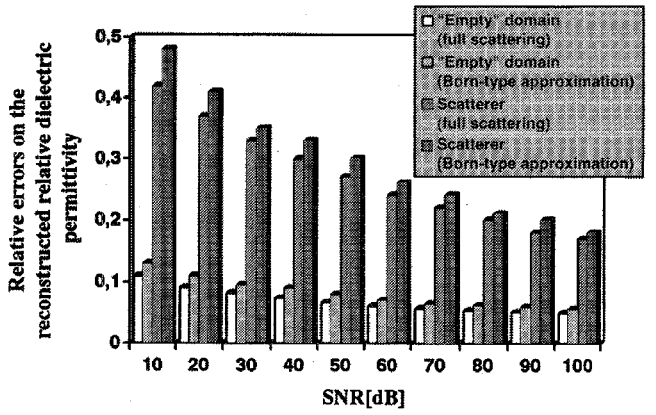

Fig. 3. Errors on the reconstructions of the dielectric permittivity for different values of the SNR. $\varepsilon_{mr} = 1.5, \varepsilon_{ar} = 2$.

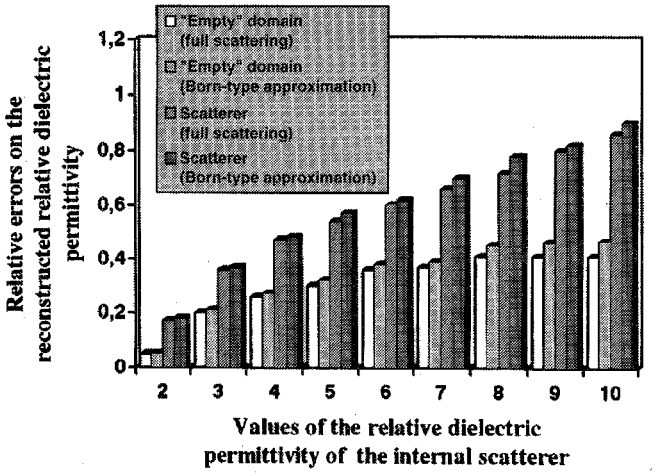

Fig. 4. Errors on the reconstruction of the dielectric permittivity versus the dielectric permittivity of the internal scatterer. $\varepsilon_{mr} = 1.5$.

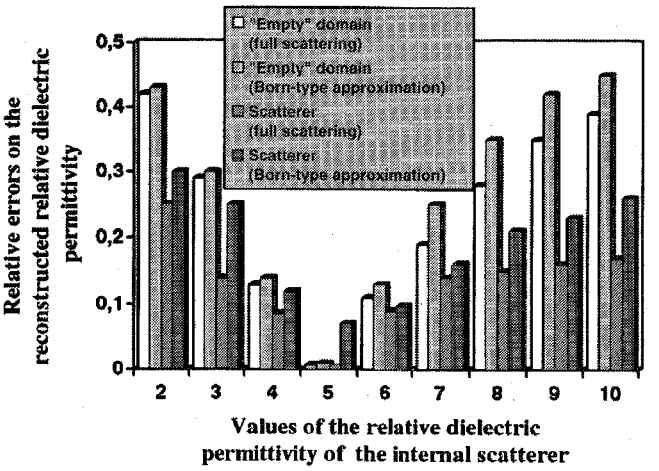

Fig. 5. Errors on the reconstruction of the dielectric permittivity versus the dielectric permittivity of the internal scatterer. $\varepsilon_{mr} = 5$.

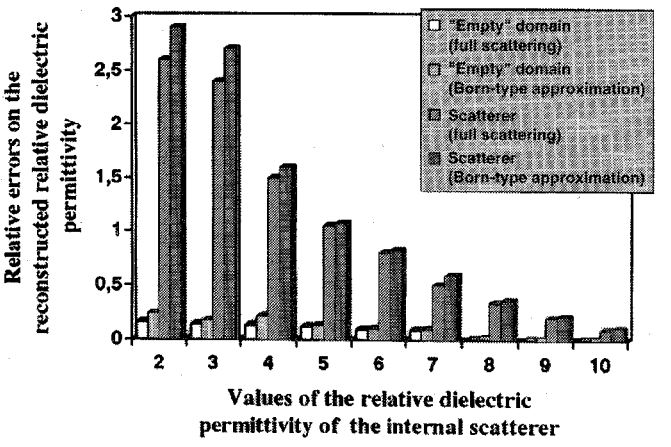

Fig. 6. Errors on the reconstruction of the dielectric permittivity versus the dielectric permittivity of the internal scatterer. $\varepsilon_{mr} = 11$.

where the scatterer is weak only with respect the surrounding medium, we consider two cases, using a basic configuration whose dielectric permittivity is $\varepsilon_{mr} = 5$ (in the first case) and $\varepsilon_{mr} = 11$ (in the second case). Fig. 5 shows the errors in the reconstructions by using the complete approach and the Born-type approximation, for the same values of the relative dielectric permittivity of the scatterer as used in Fig. 4 and for a dielectric permittivity of the "empty" domain $\varepsilon_{mr} = 5$.

For a dielectric permittivity of the "empty" domain $\varepsilon_{mr} = 11$, the errors on the reconstructions for the same values of the relative dielectric permittivity of the scatterer are those given in Fig. 6.

Figs. 4–6 show that as occurs when the classic Born approximation is applied, the Born-type approximation gives better results in the cases where the scatterer is weak with respect to the surrounding medium represented by the part of the basic structure contained in the investigation domain. The three figures point out, however, that even when the complete approach is used, the errors on the reconstructions of both the "empty" domain and the scatterer increase, as the difference between the relative permittivity values of the "empty" domain and of the scatterer increases. In this case, too, the relative errors for the approximate approach are not much larger than those related to the complete version of the approach.

IV. Numerical Simulation

To evaluate the capabilities of the proposed approach in reconstructing biological bodies, let us consider, as a test case, a schematized model of the human thorax (Fig. 7). This model is the same as used by Broquetas *et al.* [33] for a different imaging purpose (i.e., application of an efficient method for differential imaging). The different organs of the human thorax can be distinguished: the heart, muscle, blood, fat, marrow, the lungs, and bone. The dielectric permittivity values are given in Table I. The structure is placed in a homogeneous and nondissipative propagation medium characterized by ε_0 and μ_0. The cross section is partitioned into 802 square subdomains (side: 1 cm). The incident wave is a TM unit uniform plane wave in a propagation direction along the negative y axis, at a frequency $f = \omega/2\pi = 434$ MHz.

The dielectric reconstruction is performed in the various steps described in the previous sections. The process starts with the numerical computations of the Green's function and of the electric field distribution in the unperturbed configuration. The results of these computations are presented in Figs. 8 and 9. In particular, Fig. 8 shows the real and imaginary parts of the computed values of the Green's function for the thorax,

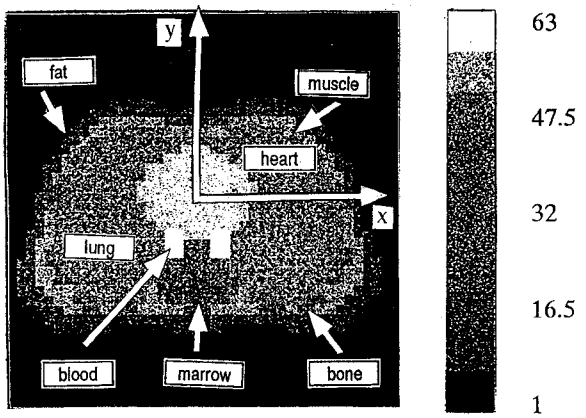

(a)

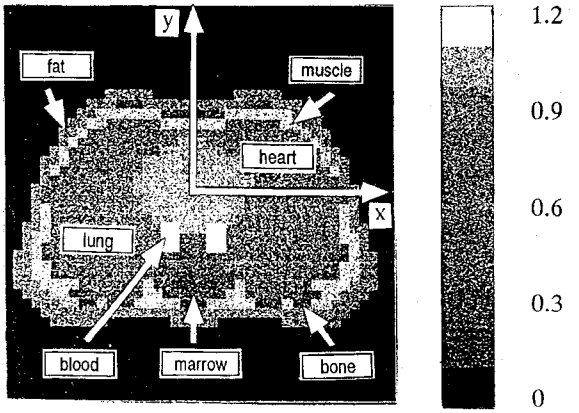

(b)

Fig. 7. Schematized human thorax [33]. Gray levels for (a) the permittivity and (b) conductivity distributions inside the thorax.

TABLE I
VALUES OF THE DIELECTRIC PERMITTIVITY AND OF THE ELECTRIC CONDUCTIVITY FOR THE TISSUES OF THE HUMAN THORAX [33] ($f = 434$ MHz)

tissue:	ε_{mr}	σ_m (S/m)
bone	8.5	0.3133
heart	56	0.92785
fat	5.5	0.7953
blood	63	1.19777
marrow	5.5	0.02892
muscle	53	0.99774
lung	36	0.60732

for a source point located in the heart region, corresponding to cell 404 (marked with a cross in Fig. 10). Fig. 9 shows the computed values of the electric field $E^{i}_{\mathrm{inc}}(x, y)$: real and imaginary parts.

We now consider a square investigation domain that includes 81 cells and an observation domain made up of 81 measurement points. For eight cells inside a lung [colored in black in Fig. 10(a)], we assume a $+15\%$ variation in the relative dielectric permittivity and a -60% variation in the electric conductivity. This configuration is called test A. Fig. 11 gives the scales used for all the original and

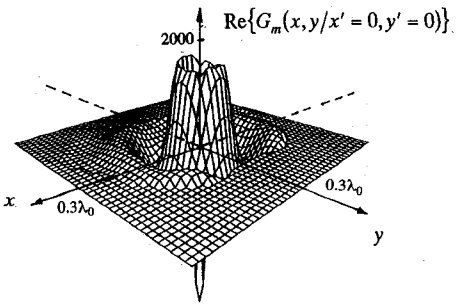

(a)

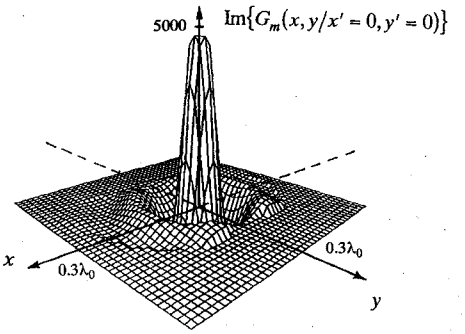

(b)

Fig. 8. Computed Green's function inside the thorax for a source point located in cell 404 (marked with a cross in Fig. 10): (a) real part; (b) imaginary part.

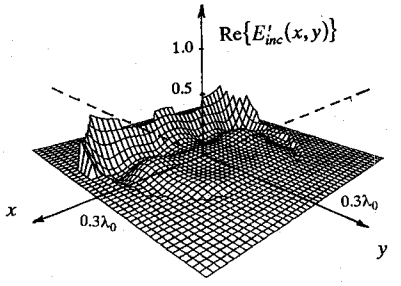

(a)

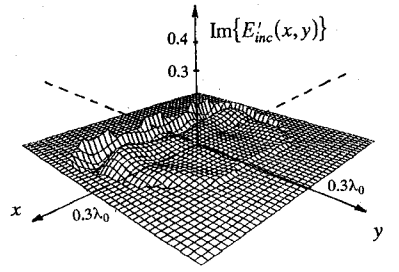

(b)

Fig. 9. Computed values of the electric field $E^{i}_{\mathrm{inc}}(x, y)$inside the thorax: (a) real part; (b) imaginary part.

reconstructed images of the dielectric permittivity and electric conductivity. Fig. 12 shows the original and reconstructed distributions of the dielectric parameters inside the investigation domain. In particular, Fig. 12(a) and (b) gives the original values and Fig. 12(c) and (d) shows the images reconstructed by using the full-scattering approach. As can be seen, the two square spots are quite distinguishable and the "empty" domain has been reconstructed quite well, although some artifacts

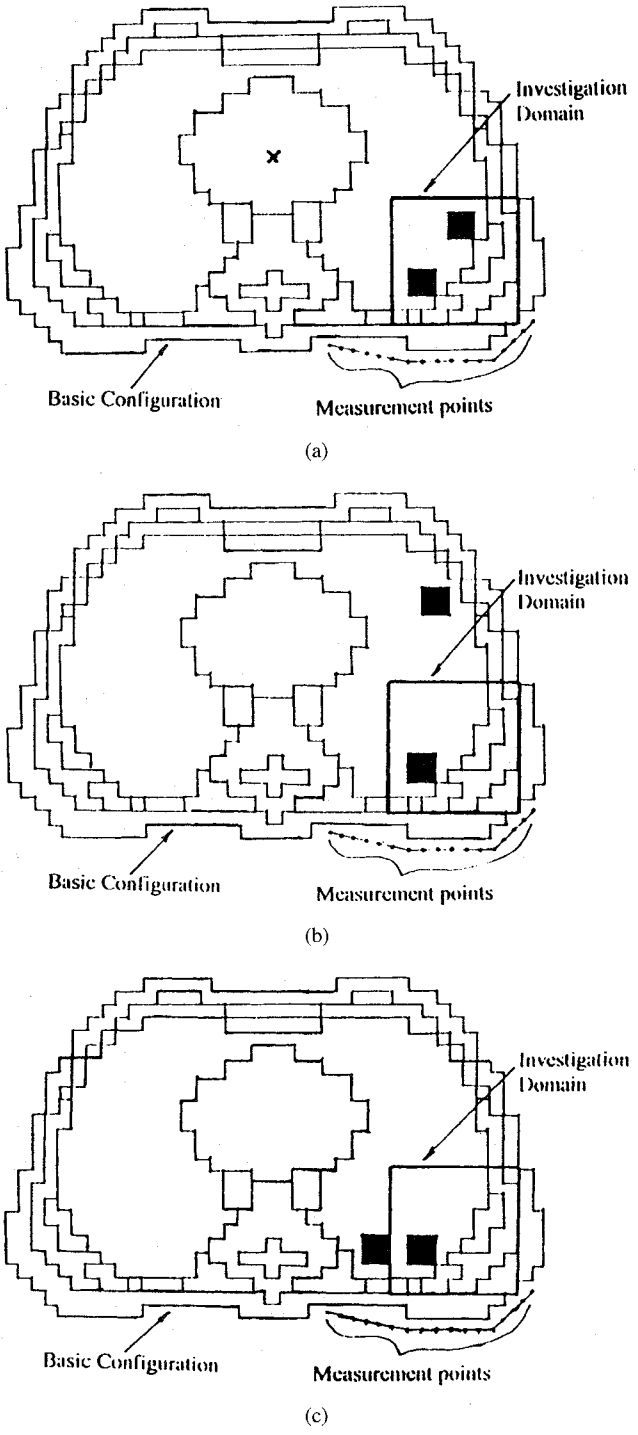

Fig. 10. Schematized human thorax. Positions of the internal scatterer in a lung: (a) test A; (b) test B; (c) test C. The cross in the heart indicates the cell containing the impulse for the computation of the Green's function shown in Fig. 8.

seem to be present, especially in the upper parts of the images (corresponding to a deeper part of the body). Of course, these are crude images that seem to contain enough information for successful applications of image-processing techniques for quality enhancement. The reconstructions obtained by using the Born-type approximation are shown in Fig. 12(e) and (f). As can be seen, there is a certain increase in the "noise," and the approximation seems to affect mainly the conductivity distribution. The quantitative errors on test A are given in

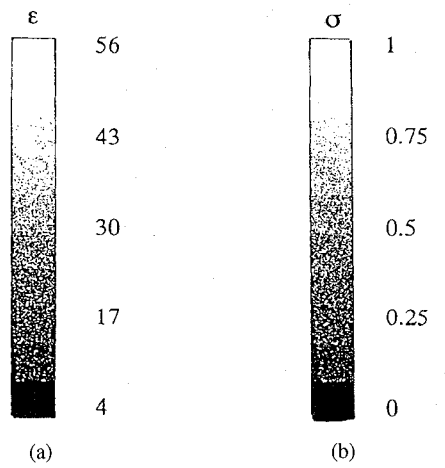

Fig. 11. Ranges of values for (a) the dielectric permittivity and (b) electric conductivity for the gray-level images of the investigation domains in Figs. 12, 13, 17, and 18.

Fig. 14(a) (for the dielectric permittivity) and (b) (for the electric conductivity). They are defined as the mean relative errors computed inside the scatterer and in the complementary part of the investigation domain. The histograms confirm that the dielectric permittivity has been reconstructed better than the electric conductivity and that there is a certain low-pass effect (associated with the minimization procedure [34]) that affects mainly the reconstruction of the scatterer.

As is well known, a multi-illumination multi-view process is of major importance to obtain accurate reconstructions in microwave imaging. To this end, for test A, we consider a two-illumination process, with two orthogonal illuminations given by plane waves. The reconstructed images of the dielectric permittivity and of the electric conductivity are then obtained by a views combination, as in [21]. They are shown in Fig. 12(g) and (h): one can notice the improvement in the reconstructions of the scatterer and of the various tissues in the investigation domain. The relative errors on the reconstructed dielectric permittivity turn out to be 2.9% for the scatterer and 2.1% for the background; the relative errors on the reconstructed electric conductivity are equal to 75% for the scatterer and to 4.8% for the background. They confirm a significant improvement in the reconstruction quality, especially for the electric conductivity.

In order to test the proposed approach under different conditions, we assume that the variations in the complex dielectric permittivity are not concentrated all in the investigation domain. To this end, we consider the configurations shown in Fig. 10(b) and (c) (called tests B and C, respectively). In these figures, four of the eight cells with different complex dielectric permittivities (with respect to the model) are outside the investigation domain and placed near it and far from it, respectively.

Fig. 13(a) and (b) shows the dielectric permittivity and the electric conductivity in the investigation domain for test B. The full-scattering reconstructions are shown in Fig. 13(c) and (d). The relative errors on the reconstructions of the dielectric permittivity and of the electric conductivity for the three tests are shown in Fig. 14. One can observe that the reconstruction error is larger if part of the scatterer is outside the investigation domain, and increases if this part is nearer the

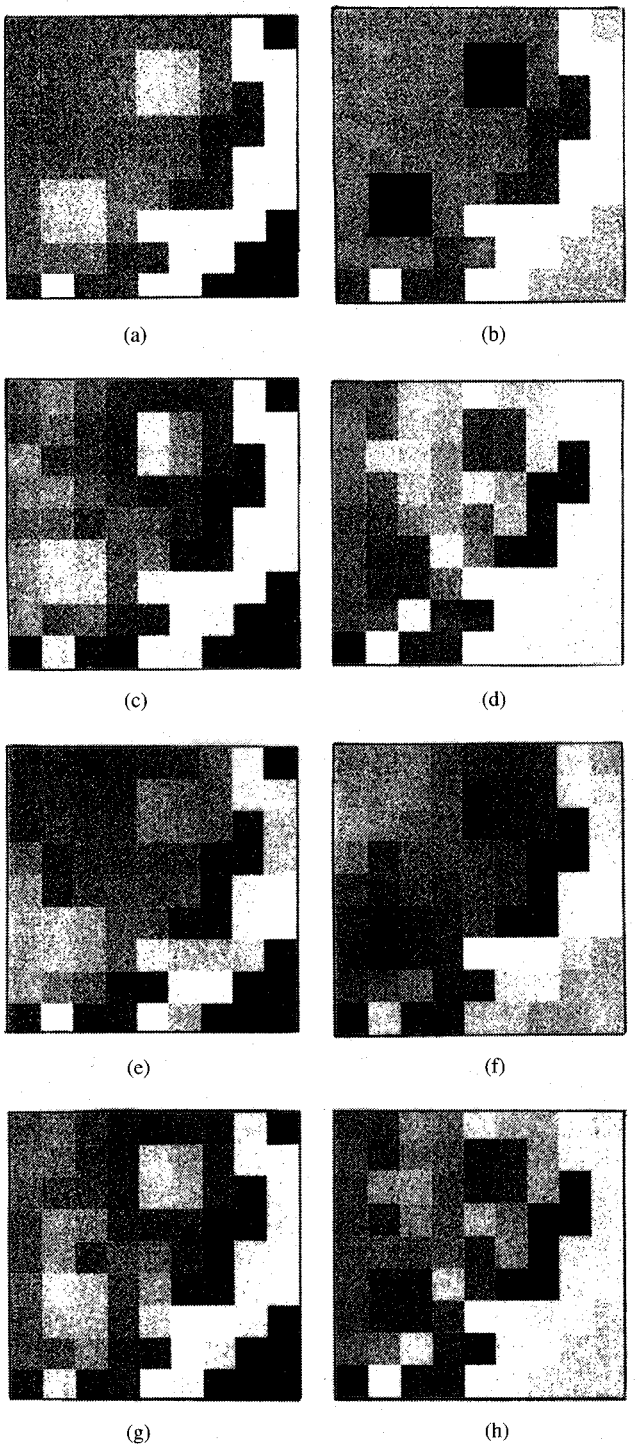

Fig. 12. Test A: (a) Dielectric permittivity of the investigation domain; (b) electric conductivity of the investigation domain; (c) reconstructed permittivity by using the complete approach; (d) reconstructed conductivity by using the complete approach; (e) reconstructed permittivity by using the Born-type approximation; (f) reconstructed conductivity by using the Born-type approximation; (g) reconstructed permittivity by using the two-view complete approach; (h) reconstructed conductivity by using the two-view complete approach.

investigation domain. The reconstructions in Figs. 13 obtained for test B, however, show that the error is well-distributed over the whole investigation domain; therefore, it does not degrade the image quality too much. Although the reconstructions of the scatterer's conductivity are characterized by rather high percent errors in all three tests, nevertheless they are

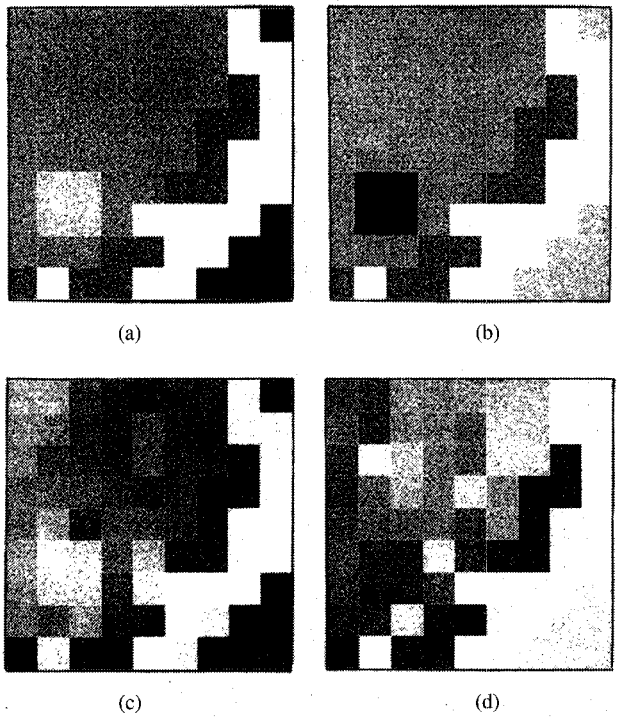

Fig. 13. Test B: (a) dielectric permittivity of the investigation domain; (b) electric conductivity of the investigation domain; (c) reconstructed permittivity by using the complete approach; (d) reconstructed conductivity by using the complete approach.

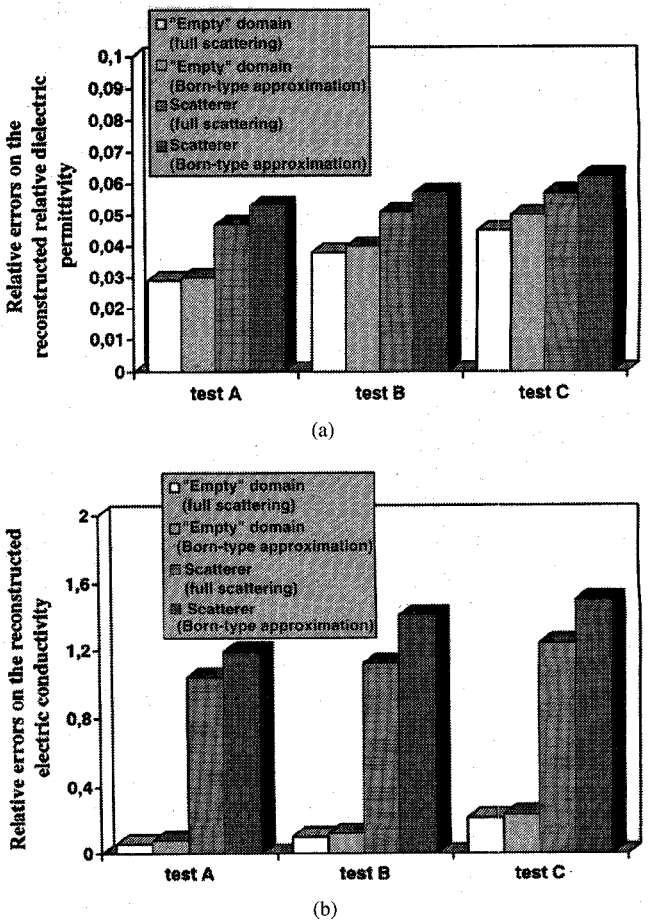

Fig. 14. Errors on the reconstructions of (a) the dielectric permittivity and (b) of the electric conductivity for tests A, B, and C.

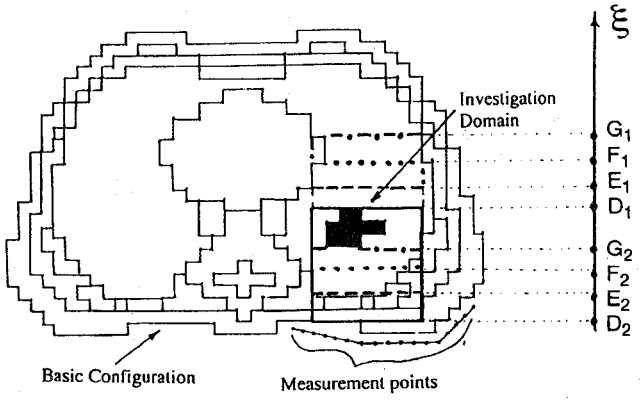

Fig. 15. Positions of the investigation domain in the schematized human thorax [33]. The investigation domain is moved toward the inner part of the thorax in the axis direction. The four positions of S_i are indicated as tests D, E, F, and G. Points X_1 and X_2 denote the projections (onto the ξ axis) of the orizontal edges of the investigation domain for test X.

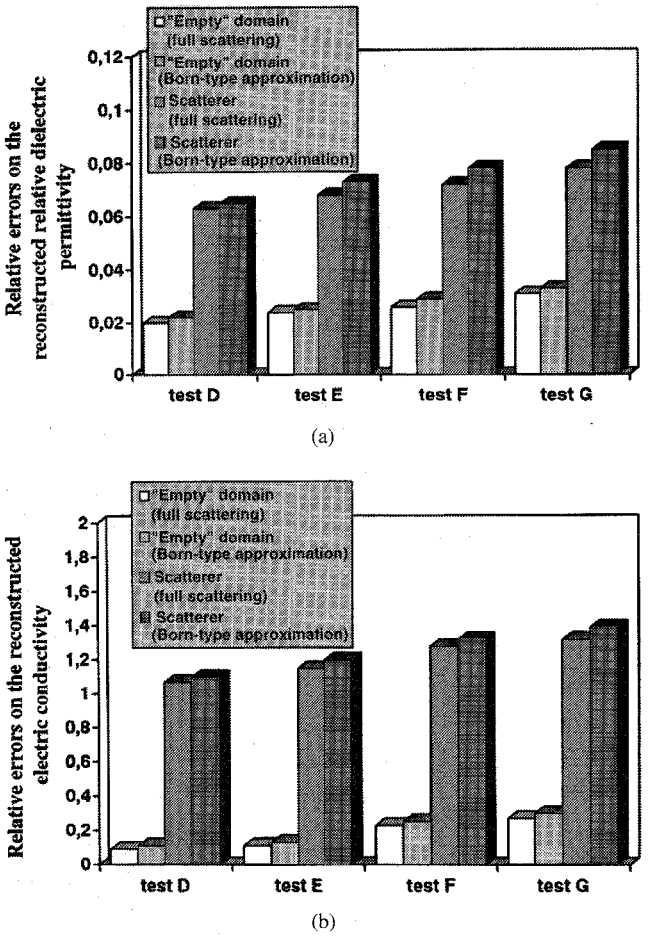

Fig. 16. Errors on the reconstructions of the dielectric permittivity (a) and of the electric conductivity (b) for tests D, E, F, and G.

satisfactory in terms of the visual contrast between the scatterer and its background.

Finally, the possibility of changing the depth of the investigation domain inside the human thorax is explored. To this end, we consider the configuration shown in Fig. 15. There are ten cells (colored in black) whose characteristics present a variation (with respect to those of a lung) that is equal to the variations assumed for the previous examples

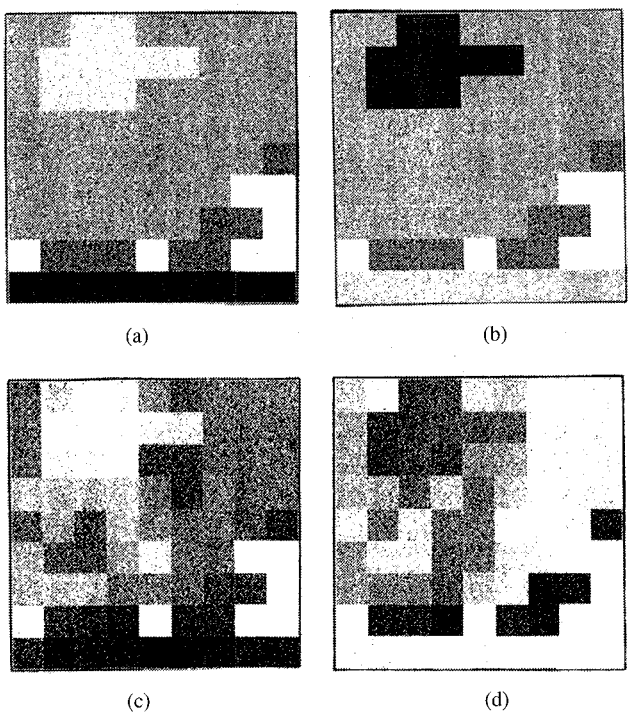

Fig. 17. Test D: (a) dielectric permittivity of the investigation domain; (b) electric conductivity of the investigation domain; (c) reconstructed permittivity by using the complete approach; (d) reconstructed conductivity by using the complete approach.

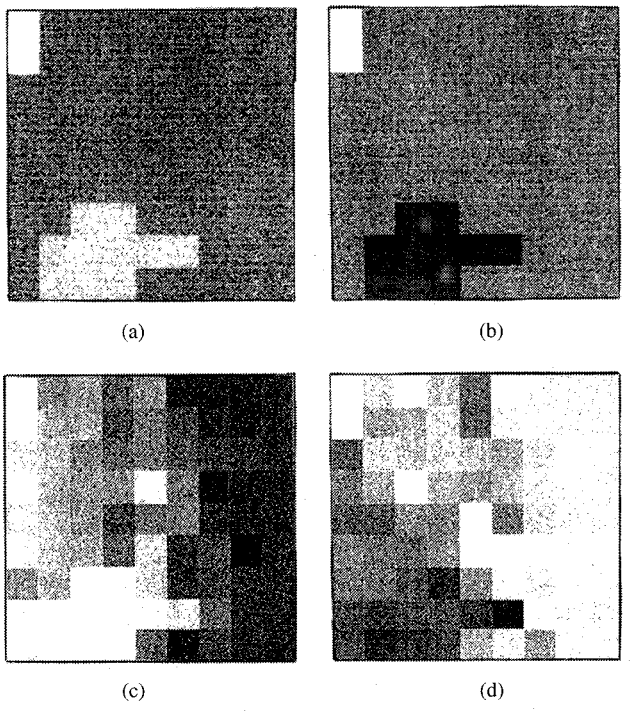

Fig. 18. Test G: (a) dielectric permittivity of the investigation domain; (b) electric conductivity of the investigation domain; (c) reconstructed permittivity by using the complete approach; (d) reconstructed conductivity by using the complete approach.

(dielectric permittivity: $\varepsilon_{ar} = 41$ and electric conductivity: $\sigma_a = 0.245\,82$).

We consider the same observation domain as used in the previous cases and an investigation domain still consisting of

81 square cells. The investigation domain is rigidly moved in the scene: in particular, we consider four positions for it (Fig. 15), obtained by shifting the investigation domain in the axis direction toward the inner part of the thorax. These tests are called tests D (less deep investigation domain), E, F, and G (deepest investigation domain), respectively. The relative errors on the reconstructions of the dielectric characteristics are shown in Fig. 16 for the four different positions of the investigation domain. As can be noticed, the farther the investigation domain from the measurement points, the larger the reconstruction error. Nevertheless, the reconstructions of the part of the basic structure contained in the investigation domain are always accurate enough and the contrast with the scatterer is always high enough. As examples, Figs. 17 and 18 give the reconstructions of the investigation domain for tests D and G, respectively. Even in Fig. 18, which corresponds to the worst reconstruction, the contrast between the scatterer and the "empty" domain can be considered acceptable.

From a computational point of view, for the reduced side of the investigation domain, the on-line computation (reconstruction) takes a few minutes on an Intel 80486-based PC and the related computational saving (once the Green's function has been computed) over moment-method-based approaches requiring that the whole cross section be considered [17] is approximately proportional to the cube of the ratio between the two problem dimensions.

V. Conclusion

A numerical approach to microwave imaging in biomedical applications has been proposed. The approach is aimed at reducing the investigation domain to a subregion inside the biological body. Starting from a model of a biological body, the method requires the off-line computation of the Green's function for the corresponding inhomogeneous structure, thus making it possible to restrict the investigation to "windows" containing a single organ or a subregion of the biological body. This results in a notable computational saving, as the reconstruction process is limited to an area of interest, without a need for reconstructing the whole body (in general, this is not a requirement). Therefore, all computational resources can be devoted to accurately reconstructing the selected region. A reconstruction technique, previously developed, is then applied. A test case has been described, using a schematized model of a the human thorax, previously considered by other authors for differential imaging. The reduced investigation domain has been moved inside the body and the possibility that an "excess of permittivity" (with respect to the *a priori* assumed model) may be present outside the test area has been considered. This has resulted in noise in the reconstructed images. One- and two-view processes have been considered, together with the application of a Born-type approximation. The possibility of applying this type of approximation is another feature of the method. In this case, the inverse scattering problem is linearized, with a notable reduction in its critical aspects, without the application of the classic Born approximation, which, due to the high contrast of the body, could not have yielded acceptable results.

The obtained reconstructions, although rather preliminary, seem to indicate the possibility of quite accurate focused imaging. Such imaging could be exploited for the development of techniques aimed at reducing the problems involved in traditional solutions of the inverse scattering problem for biological bodies. Without the extensive use of *a priori* information, this problem turns out to be intrinsically ill-posed and difficult to treat in a satisfactory way. In our opinion, the combination of different diagnostic techniques and the use of image-processing procedures may make microwave imaging a competitive diagnostic technique, or, at least, a good complementary technique to existing diagnostic methodologies.

References

[1] L. E. Larsen and J. H. Jacobi, Eds., *Medical Applications of Microwave Imaging*. New York: IEEE Press, 1986.

[2] C. Pichot, L. Jofre, G. Perronet, and J. C. Bolomey, "Active microwave imaging of inhomogeneous bodies," *IEEE Trans. Antennas Propagat.*, vol AP-33, pp. 416–425, 1985.

[3] M. J. Hagmann and R. L. Levine, "Procedures for noninvasive electromagnetic property and dosimetry measurements," *IEEE Trans. Antennas Propagat.*, vol. 38, pp. 99–106, 1990.

[4] J. C. Bolomey, "Recent European developments in active microwave imaging for industrial, scientific, and medical applications," *IEEE Trans. Microwave Theory Tech.*, vol. 37, pp. 2109–2117, 1989.

[5] A. V. Vorst, "Microwave bioelectromagnetics in Europe," in *Proc. IEEE Microwave Symp.*, Atlanta, GA, June 1993.

[6] A. Broquetas, L. Mallorqui, and L. Jofre, "Medical applications of microwave imaging," in *Proc. Workshop on Inverse Scattering and Microwave Imaging, 25th European Microwave Conf.*, Bologna, Italy, 1995, p. 77.

[7] T. C. Guo and W. W. Guo, "3-D dielectric imaging by inverse scattering with resolution unlimited by wavelength," in *Annu. Rep. Conf. Electrical Insulation and Dielectric Phenomena*, Leesburg, VA, 1989, pp. 65–74.

[8] J. C. Bolomey, A. Broquetas, P. Cottis, J. Van Dijk, and G. Gaboriaud, "Microwave imaging capabilities for noninvasive thermometry," *COMAC-BME Hyperthermia Bull.*, no. 2, pp. 14–17, 1990.

[9] J. Devaney, "A computer simulation study of diffraction tomography," *IEEE Trans. Biomed. Eng.*, vol. BME-30, pp. 377–386, 1983.

[10] T. C. Guo and W. W. Guo, "Computation of electromagnetic wave scattering from an arbitrary three-dimensional inhomogeneous dielectric object," *IEEE Trans. Magn.*, vol. 25, pp. 2872–2874, 1989.

[11] M. M. Ney, A. M. Smith, and S. S. Stuchly, "A solution of electromagnetic imaging using pseudoinverse transformation," *IEEE Trans. Med. Imaging*, vol. MI-3, pp. 155–162, 1984.

[12] S. Caorsi, G. L. Gragnani, and M. Pastorino, "A multiview microwave imaging system for two-dimensional penetrable objects," *IEEE Trans. Microwave Theory Tech.*, vol. 39, pp. 845–851, 1991.

[13] A. N. Datta and B. Bandyopadhyay, "Nonlinear extension to a moment method iterative reconstruction algorithm for microwave tomography," *Proc. IEEE*, vol. 74, pp. 604–606, 1986.

[14] N. Joachimowicz, C. Pichot, and J. P. Hugonin, "Inverse scattering: An iterative numerical method for electromagnetic imaging," *IEEE Trans. Antennas Propagat.*, vol. 39, pp. 1742–1752, 1991.

[15] D. K Ghodgaonkar, O. P. Gandhi, and M. J. Hagmann, "Estimation of complex permittivities of three-dimensional inhomogeneous biological bodies," *IEEE Trans. Microwave Theory Tech.*, vol. MTT-31, pp. 442–446, 1983.

[16] C. Pichot, "Spectral and spatial-domain technique for microwave imaging," in *Proc. Workshop on Inverse Scattering and Microwave Imaging, 25th European Microwave Conf.*, Bologna, Italy, 1995, pp. 85–90.

[17] S. Caorsi, G. L. Gragnani, and M. Pastorino, "Reconstruction of dielectric permittivity distributions in arbitrary 2-D inhomogeneous biological bodies by a multiview microwave numerical method," *IEEE Trans. Med. Imaging*, vol. 12, pp. 232–239, 1993.

[18] W. C. Chew, Y. M. Wang, G. Otto, D. Lesselier, and J. C. Bolomey, "On the inverse source method of solving inverse scattering problems," *Inverse Problems*, vol. 10, pp. 547–553, 1994.

[19] J. J. Mallorquì and A. Broquetas, "Microwave inverse scattering: Biomedical and industrial applications," in *Proc. Progress in Electromagnetic Research Symp.*, Seattle, WA, 1995.

[20] C. Pichot and P. Lobel, "Gauss-Newton and gradient methods for microwave tomography," in *Proc. Meet. on Inverse Problems in Medical Imaging and NDT*, to be held in Oberwolfach, Germany, 1996.

[21] S. Caorsi, G. L. Gragnani, S. Medicina, M. Pastorino, and G. A. Pinto, "A Gibbs random field-based active electromagnetic method for noninvasive diagnostics in biomedical applications," *Radio Sci.*, vol. 30, pp. 291–301, 1995.
[22] ——, "A new space-domain microwave imaging approach to detecting inhomogeneous dielectric objects," in *Proc. 24th European Microwave Conf.*, Cannes, France, 1994, pp. 590–595.
[23] P. M. Morse and H. Feshback, *Method of Theoretical Physics*. New York: McGraw-Hill, 1953.
[24] C. T. Tai, *Dyadic Green Function in Electromagnetic Theory*. New York, IEEE Press, 1994.
[25] W. C. Chew, *Waves and Fields in Inhomogeneous Media*. New York, IEEE Press, 1995.
[26] W. C. Chew and Y. M. Wang, "Reconstruction of two-dimensional permittivity distribution using the distorted Born iterative method," *IEEE Trans. Med. Imaging*, vol. 9, pp. 218–225, 1990.
[27] A. G. Tijhuis and F. E. van Vliet, "Practical consideartions for two-dimensional velocity inversion using the distorted-wave Born iterative technique," in *Proc. XXIVth URSI General Assembly*, Kyoto, Japan, 1993, p. 83.
[28] M. Slaney, A. C. Kak, and L. E. Larsen, "Limitation of imaging with first-order diffraction tomography," *IEEE Trans. Microwave Theory Tech.*, vol. MTT-32, pp. 860–873, 1984.
[29] R. E. Kleinman and P. M. van den Berg, "Two-dimensional location and shape reconstruction," *Radio Sci.*, vol. 29, p. 1157, 1994.
[30] A. D. Yaghjian, "Electric dyadic Green's functions in source region," *Proc. IEEE*, vol. 68, pp. 248–263, 1980.
[31] R. F. Harrington, *Field Computation by Moment Method*. New York: Macmillan, 1968.
[32] R. E. Kleinman, G. F. Roach, and P. M. van den Berg, "Convergent Born series for large refractive indices," *J. Opt. Soc. Am. A*, vol. 7, pp. 890–897, 1990.
[33] A. Broquetas, J. J. Mallorquì, J. M. Rius, L. Jofre, and A. Cardama, "Active microwave sensing of highly contrasted dielectric bodies," *J. Electromagnetic Wave and Appl.*, vol. 7, pp. 1439–1453, 1993.
[34] S. Caorsi, S. Ciaramella, G. L. Gragnani, and M. Pastorino, "On the use of regularization techniques in numerical inverse-scattering solutions for microwave imaging applications," *IEEE Trans. Microwave Theory Tech.*, vol. 43, pp. 632–640, 1995.

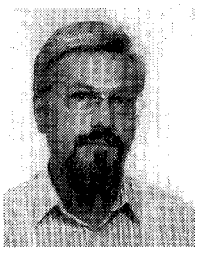

Salvatore Caorsi received the "laurea" degree in electronic engineering from the University of Genoa, Genoa, Italy, in 1973.

After graduation he remained at the university as a Researcher, and since 1976 he has been Associate Professor of Antennas and Propagation at the Department of Biophysical and Electronic Engineering of the University of Genoa. In 1985 he also assumed the title of Professor of Fundamentals of Remote Sensing. Since 1994, he has been full Professor of Electromagnetic Compatibility at the Department of Electronics of the University of Pavia, Italy. He is the Past-President and founding member of the Inter-university Research Center for Interactions Between Electromagnetic Fields and Biological Systems (ICEMB). His primary activities are focused on applications of electromagnetic fields to telecommunications, artificial vision and remote sensing, biology, and medicine. In particular, he is working on research projects concerning microwave hyperthermia and radiometry in oncological therapy; numerical methods for solving electromagnetic problems; wave propagation in presence of nonlinear media; and inverse scattering and microwave imaging.

Mr. Caorsi is a member of the Associazione Elettrotecnica ed Elettronica Italiana (AEI), the European Bioelectromagnetism Association (EBEA) and the European Society for Hyperthermic Oncology (ESHO).

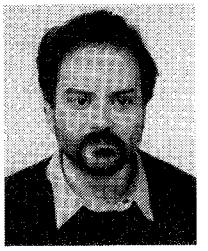

Gian Luigi Gragnani (M'89) received the "laurea" degree in electronic engineering from the University of Genoa, Genoa, Italy, in 1985.

In the same year, he joined the Applied Electromagnetics Group in the Department of Biophysical and Electronic Engineering (DIBE) and subsequently he has cooperated with the Inter-university Research Center for Interactions Between Electromagnetic Fields and Biological Systems. Since 1989 he has been responsible for the DIBE Applied Electromagnetics Laboratory. His primary research interests are in the field of electromagnetic scattering (both direct and inverse). In particular, he is engaged in research work on numerical methods for addressing electromagnetic problems, on microwave imaging, on biomedical applications of electromagnetic fields (especially microwave hyperthermia and radiometry), and on electromagnetic compatibility.

Mr. Gragnani is a member of the Associazione Elettrotecnica ed Elettronica Italiana (AEI), and of the European Bioelectromagnetism Association (EBEA).

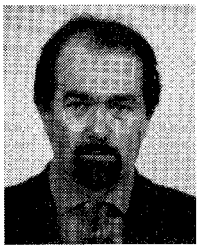

Matteo Pastorino (M'90–SM'96) received the "laurea" degree in electronic engineering from the University of Genoa, Genoa, Italy, in 1987 and the Ph.D. degree in electronics and computer science from the same university in 1992.

Since 1987, he has cooperated in the activities of the Applied Electromagnetics Group and, since the year it was established, in the activities of the Inter-University Research Center for Interactions Between Electromagnetic Fields and Biological Systems. At present he is an Assistant Professor of Electromagnetic Fields in the Department of Biophysical and Electronic Engineering and, since 1995, he has taught university courses of Electromagnetic Fields 1 and Remote Sensing and Electromagnetic Diagnostic. His main research interests are in electromagnetic direct and inverse scattering, microwave imaging, wave propagation in presence of nonlinear media, and in numerical methods in electromagnetism. He is also working on research projects concerning biomedical applications of electromagnetic fields.

Dr. Pastorino is a member of the Associazione Elettrotecnica ed Elettronica Italiana (AEI) and the European Bioelectromagnetism Association (EBEA).

Mauro Rebagliati received the "laurea" degree "summa cum laude" in electronic engineering from the University of Genoa, Italy, in 1995.

Since graduation, he has collaborated with the activities of Electromagnetics Group of the Department of Biophysical and Electronic Engineering at the University of Genoa. His main interests are in the fields of inverse scattering and microwave imaging.